Axial Crush of Metallic and Hybrid Energy Absorbing Thin-walled Tubes with Polygonal Cross-sections: Numerical Analysis

S.A. Yousefsani[1], J. Rezaeepazhand[2,*] , S.A. Maghami[3]

[1,3] Student, [2] Professor, Department of Mechanical Engineering, Ferdowsi University of Mashhad, Mashhad, Iran

jrezaeep@um.ac.ir

Abstract

Material properties and geometry are two important design parameters which their effects should be considered in a crashworthiness analysis. In this paper, the axial impact of metallic and hybrid energy absorbing thin-walled tubes with poly-gonal cross-section is simulated using LS-DYNA software. The combined effects of changing the geometry and material properties on the mass specific energy absorption (MSEA) as well as the mean and maximum crush forces are investigated. To compare the results, all metallic tubes have identical thickness, length, and circumference. The hybrid tubes are made of the same metallic tubes which are reinforced with special composite overlays. These materials are intentionally selected in such a way that the effects of yield strength and Young's modulus can be separately investigated. The results show that, in contrast with the current belief, there are some metallic and hybrid tubes with non- circular cross-section shapes, which have better mass specific energy absorption capabilities than the circular ones during the impact.

Keywords: axial crush, energy absorbing, hybrid thin-walled tubes, mean and maximum crush forces.

1. Introduction

Heretofore, automotive industries have developed their products to make them safer and more convenient. Researchers have tried to design the structures such a way to decrease the damages that imperil the passengers' lives. Thus, clearly, the improvement of structural crashworthiness is a noteworthy problem. One of the important aspects of studying the crashworthiness is the ability to absorb the impact energy. The main purpose of strengthening a structure is to dissipate the crush energy in order to reduce the damages.

The crush energy can be absorbed during the deformation and destruction of some certain components fitted in proper locations. The metallic thin-walled tubes seem to be suitable for this purpose due to their low cost, easy fabrication, and high efficiency in absorbing energy. Moreover, using composite materials and designing the best shapes and dimensions can improve the efficiency of these components.

Various parameters, such as material properties, cross-sectional geometries, thickness, stacking sequences, and the speed of collision can affect the energy absorption capability of hybrid tubes. During the impact of hybrid tubes, the crush energy can be absorbed due to plastic deformation of metallic layer, fiber crushing, matrix breaking, fiber deboning, and also friction. However, during the crush of metallic tubes, this energy is mainly absorbed due to plastic deformation and friction. Abramowicz and Jones [1-3] have performed several experiments on the impact of thin-walled tubes of circular and square cross-section with different sizes. Axial crush of circular aluminum tubes was experimentally and numerically investigated by Al Galib and Limam [4]. The effects of the wall thickness of metallic square-shaped tubes and material properties of the mild and high strength steels on the energy absorption capability of tubes were studied by Tai et al. [5].

Mamalis et al. [6] studied the energy absorption capabilities of the bi-material tubes. The energy absorption of the aluminum tubes reinforced by composite laminates under axial compression and bending are studied by Shin et al. [7]. Studying the mechanism of a buckling initiator and its influences on the energy absorption capability of composites has been conducted by Thuis et al. [8] and Yang et al. [9]. Moreover, Sultan Aljibori et al. [10] investigated the effect of geometry on the energy absorption and modes of failure of composite conical shells using nonlinear dynamic analysis.

Some numerical and experimental researches on the axial crushing of composite tubes and their brittle fracture modes in a static progressive crush have been carried out by Huang [11]. The effects of delimitation during the first and second modes of failure of hybrid composite tubes on their crushing behavior are studied by Qasemnejad et al. [12]. Furthermore, other researches ([13] and [14]) have shown that the hybrid thin-walled tubes are very efficient due to their higher strength to weight ratio. Although a considerable amount of studies has been devoted to crush of thin-walled tubes with different materials or geometries, little attention has been focused on the combined effects of these two parameters.

In this paper, the axial crush of metallic and hybrid energy absorbing thin-walled tubes has been simulated. In order to study the effects of material properties on the impact behavior of the tubes, four different metals and three different composite overlays with special mechanical properties are considered. The comparison between results is performed for several conditions of mechanical properties in which the effects of making some meaningful changes in Young's module and yield strengths are studied. Furthermore, some special cross-section shapes for both metallic and hybrid tubes are selected to investigate the effects of change in geometry on the energy absorption capability of these tubes.

2. Material Models and Mechanical Properties

The material model No. 24 of the LS-DYNA material library has been used to model the mechanical properties of the metallic tubes. This material model demonstrates the piecewise-linear-plasticity behavior, which includes the strain rate dependency. For modeling the composite laminates, the material model No. 54 has been used, which represents an orthotropic material [15].

To study the effects of cross-sectional geometry and the mechanical properties of materials for the metallic tubes, four various metals included two aluminum and two steel alloys are selected. It should be noted that, AA 2024-T4 and mild steel have the same yield stresses and different Young's module. On the other hand, mild steel and high strength steel have identical Young's module and different yield stresses. Moreover, AA 6063-T52 has the poorest mechanical properties relative to others. The mechanical properties of these metals are presented in table 1, and their plastic stress-plastic strain diagrams are also illustrated in figure 1.
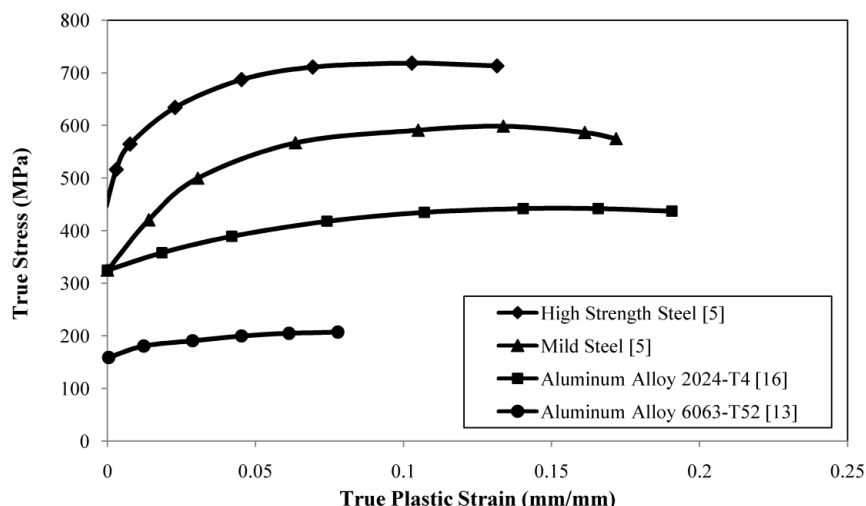

Fig1. True stress-true plastic strain curves of metals

To find out reinforcing effects, the second part of the study includes the simulation of axial crush of an aluminum tube and three hybrid tubes. These hybrid tubes are made of the same metallic layers which are

overlaid with three different composite laminates. Note that in all hybrid tubes, the metallic layer is made of aluminum (AA 6063-T52) due to its wide applications in the automotive industries. On the other hand, Aramid epoxy is chosen as an overlay because of its low longitudinal Young's modulus, low longitudinal compressive strength, and high longitudinal tensile strength in contrast with Boron epoxy, which has high longitudinal Young's modulus,

high longitudinal compressive strength, and low longitudinal tensile strength. Furthermore, Carbon PEEK is selected due to its mean properties. The mechanical properties of the aluminum tube [13] and composite laminates [17] are listed in tables 1 and 2, respectively. Although these composite materials are expensive, they are intentionally selected to study the effects of mechanical properties.

Table 1, Mechanical properties of metals

Property (unit)	Aluminum Alloy 6063-T52 [13]	Aluminum Alloy 2024-T4 [16]	Mild Steel [5]	High Strength Steel [5]
Density ρ (kg/mm^3)	2.7×10^{-6}	2.78×10^{-6}	7.82×10^{-6}	7.82×10^{-6}
Young's Modulus E (GPa)	69	73.1	207.2	207.2
Yield Stress $\sigma_{y.p}$ (MPa)	160	324	325	446
Poisson's Ratio v	0.33	0.33	0.33	0.33

Table 2, Mechanical properties of each composite lamina [17]

Property (unit)	Aramid epoxy	Boron epoxy	Carbon PEEK
Density ρ (kg/mm^3)	1.32×10^{-6}	2.1×10^{-6}	1.6×10^{-6}
Longitudinal Young's modulus E_1 (GPa)	95	210	140
Transverse Young's modulus E_2 (GPa)	5.1	19	10
In-plane shear modulus G_{12} (GPa)	1.8	4.8	5.1
Minor Poisson's ratio v_{21}	0.0183	0.019	0.0214
Longitudinal tensile strength X_{LT} (MPa)	2500	1300	2100
Longitudinal compressive strength X_{LC} (MPa)	300	2000	1200
Transverse tensile strength X_{TT} (MPa)	30	70	75
Transverse compressive strength X_{TC} (MPa)	130	300	250
In-plane shear strength X_{LTS} (MPa)	30	80	160

3. Composite Laminates Failure Criteria

Most common failure modes in composite laminates are fiber breakage, matrix cracking, fiber debonding, and delamination. The behavior of the first two modes, which depends on the in-plane stresses, can be explained using the thin shell theory [14]. For deboning and delaminating modes, the 3D representation of the constitutive equations and micro-mechanical modeling of the interface between layers must be considered, respectively [14].

Material model No. 54 uses either Chang-Chang or Tsai-Wu failure criteria [15]. Chang-Chang failure criterion not only includes the tensile and compressive failures of fiber and matrix, but also can

represent the non-linear shear stress-strain behavior of the lamina. In this research, the Chang-Chang failure criterion is used. However, LS-DYNA software uses slightly modified post-failure conditions for the material model No. 54 [15].

To clarify how the failure criteria are employed in the material model No. 54 in order to indicate the laminas failure modes during the impact, four failure conditions including the tensile and compressive failures of the fiber and matrix are considered in this model. Based on the total failure hypothesis of the laminas, the failure occurs once at least one of the mentioned failure conditions takes place. In such conditions (after the failure), both the strength and stiffness of the failed lamina are set equal to zero. These failure conditions are clarified as follows [14]:

Tensile fiber ruptures ($\sigma_f > 0$):

$$\left(\frac{\sigma_f}{X_{LT}}\right)^2 + \xi\left(\frac{\sigma_{fm}}{X_{LTS}}\right) - 1 \begin{cases} \geq 0 \text{ Failed} \\ < 0 \text{ Elastic} \end{cases} \qquad (1)$$

In the inequality above for the tensile fiber rupture, $0 \leq \xi \leq 1$ is a weighting factor for the shear term. In this case, for the failed lamina we have $E_1 = E_2 = G_{12} = v_{12} = v_{21} = 0$.

Compressive fiber failure or fiber buckling ($\sigma_f < 0$):

$$\left(\frac{\sigma_f}{X_{LC}}\right)^2 - 1 \begin{cases} \geq 0 \text{ Failed} \\ < 0 \text{ Elastic} \end{cases} \qquad (2)$$

In this case, for the failed lamina we have
$E_1 = v_{12} = v_{21} = 0$.

Tensile matrix failure or matrix cracking due to in-plane shear and transverse tension ($\sigma_m > 0$):

$$\left(\frac{\sigma_m}{X_{CT}}\right)^2 + \left(\frac{\sigma_{fm}}{X_{LTS}}\right)^2 - 1 \begin{cases} \geq 0 \text{ Failed} \\ < 0 \text{ Elastic} \end{cases} \qquad (3)$$

In this case, for the failed lamina we have
$E_2 = v_{21} = G_{12} = 0$.

Compressive matrix failure or matrix cracking due to in-plane shear and transverse compression ($\sigma_m < 0$):

$$\left(\frac{\sigma_m}{2X_{LTS}}\right)^2 + \left[\left(\frac{X_{TC}}{2X_{LTS}}\right)^2 - 1\right]\frac{\sigma_m}{X_{TC}} + \left(\frac{\sigma_{fm}}{X_{LTS}}\right)^2 - 1 \begin{cases} \geq 0 \text{ Failed} \\ < 0 \text{ Elastic} \end{cases}$$
$$(4)$$

In this case, for the failed lamina we have
$E_2 = v_{12} = v_{21} = G_{12} = 0$.

In these inequalities, σ_f, σ_m, and σ_{fm} represent the stress in fiber direction, the stress in perpendicular-to-the fiber direction, and the shear stress in the lamina plane, respectively. Moreover, all other parameters are defined as introduced in Table 2. The presented

relations must be applied to each lamina to investigate if it is failed during the impact or not.

In addition to the aforementioned failure criteria, some other limiting parameters such as the maximum strain for fiber tension and compression (i.e. DFAILT and DFAILC, respectively) must be specified and set in the material model No. 54. These parameters are selected as what presented in Ref [14] and are listed in Table 3.

4. Geometry Modeling

All tubes have equal length of 100 mm and regular cross-sections, such as circle or polygons with $n = 3, 4, \ldots, 8$, where n indicates the number of sides for each shape. The metallic tubes and metallic layers of hybrid tubes have equal circumferences of 100 mm. All the metallic tubes have the thickness of 1.6 mm; while, the hybrid tubes consist of the similar metallic tubes overlapped with 1.9 mm thick composite laminates. The composite overlays are made of four-layered angle-ply $(\pm45)_2$ laminate. The results of simulation for polygons with $n > 8$ have shown no significant differences in comparison with circle-shaped ones because their shapes are close to a circle.

As illustrated in figure 2, the inner wall (aluminum layer) and outer wall (composite overlay) are shown with different colors. In order to lead the folding pattern during the axial crush, 0.3 mm depression is imposed to a circumferential row of elements to form a buckling initiator. Figure 3 shows the position and dimensions of this buckling initiator, schematically.

Table 3, Strain limiting and failure parameters [14]

| Parameter	Description	Value
DFAILT	Maximum strain for fiber tension	2.3 %
DFAILC	Maximum strain for fiber compression	1.4 %
FBRT	Reduction factor for tensile strength in the fiber direction after matrix failure	1.0
YCFAC	Reduction factor for compressive strength in the fiber direction after matrix failure	3.0
TFAIL	Time step quotient	0.25
SOFT	Softening factor for element crush front	0.75
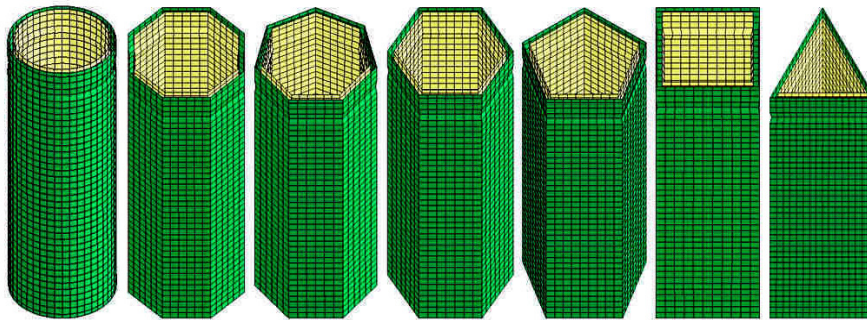
Fig2. Geometric models of hybrid tubes

5. Finite Element Model and Boundary Condition

As shown in figure 3, the rigid wall with constant speed of 100 mm/s, in the absence of gravitational force, crushes the tube from the top, and causes it to fold and absorb energy. Since the impact velocity is assumed to be constant, and the gravity does not act on the specimen, the results are independent of the mass of the rigid wall. To make the static crushing conditions and eliminate the effects of inertia, the density of both aluminum and composite layers is multiplied by 1000 [14].

The Belytschko-Tsay 4-node shell element which is located at the mid-plane of each wall is used to model the aluminum and composite layers in tubes. This element has 2 and 4 integration points through the thickness for aluminum and composite layers, respectively. According to mesh refinement and the recommendation of previous study [14], the element size is set to be 2.5 mm for both aluminum and composite walls.

To apply the contact conditions to hybrid tubes, three contact algorithms are employed. The CTNO (CONTACT_TIEBREAK_NODES_ONLY) can be imposed to model the bonding between aluminum and composite layers. The CTNO, in fact, ties these layers together, and creates a contact surface with a coefficient of friction. This contact algorithm takes both the shear and normal interfacial forces into account, and follows the tiebreak criterion as below [15]:

$$\left(\frac{f_n}{\text{NFLF}}\right)^2 + \left(\frac{f_s}{\text{SFLF}}\right)^2 \geq 1 \tag{5}$$

in which f_n and f_s represent the normal and shear forces at the interface; while the NFLF and SFLF indicate the normal and shear forces limits at the bond failure [15].

Tiebreak failure occurs once the left side of relation (5) exceeds the unit. Han et al. [18] have demonstrated that the variation of the failure bond limits has minor effects on the energy absorption capability of tubes and the folding pattern. Considering what Han et al. [18] have indicated, the authenticity of modeling of the axial impact of the verification hybrid tube was done without considering this contact algorithm between the metallic and composite lay-ups.

As it will be shown, the validation graph of presented results in comparison with those reported by Ref. [14] demonstrates no significant offset in folding patterns and the energy absorption capability of the tube by ignoring this contact algorithm. Therefore, in order to reduce the computational cost, in the remainder of present study, this contact algorithm is regarded.

To prevent the interpenetration between the continuous folds of the composite and aluminum layers, CASS (CONTACT_AUTOMATIC_SINGLE_SURFACE) with the coefficient of friction of 0.3 is used. CANTS (CONTACT_AUTOMATIC_NODES_TO_SURFACE) is employed to simulate the interfacial conditions between the rigid wall and the hybrid tube with the coefficient of friction of 0.9. Similarly, the CASS and the CANTS with the same coefficients of friction, as stated before, are used to provide contact conditions for the metallic tubes.
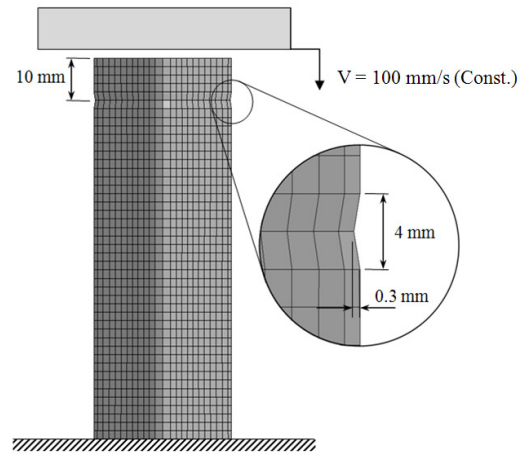
Fig3. Position and dimensions of buckling initiator

Maximum and mean crush forces and mass specific energy absorption (MSEA), which can be obtained using the force-deformation (*F-D*) diagram, are the important parameters for comparing the results of the crush simulation. Energy absorbing capacity can be calculated as the MSEA, which is the crush energy per unit deformed mass. This energy is absorbed through the folding of the tube.

The equivalent average constant force which the tube can sustain is called the mean force. The more energy can be absorbed during the impact when the greater mean force becomes sustained. Furthermore, the maximum force represents the peek crush load imposed to the tube at the beginning of the folding process. The force-deformation diagram can be drawn by combining and cross plotting the force-time and deformation-time diagrams.

Figure 4 shows the important characteristics of a sample *F-D* diagram. It should be noted that the absorbed energy can be calculated as the area under the *F-D* diagram for a specified length of deformation.

The mass specific energy absorption can be calculated as follows [5]:

$$MSEA = E_T (\Delta M)^{-1} = E_T (\rho A \Delta L)^{-1} \qquad (6)$$

In this relation, MSEA, E_T, and ΔM represent the mass specific energy absorption, total absorbed energy, and the deformed mass, respectively. For all tubes, the deformed length, ΔL, is equal to 70 mm. The mean crushing force, P_{mean}, which is the absorbed energy per unit length, can be obtained as follows:

$$P_{mean} = \frac{\int p d\delta}{\Delta L} \qquad (7)$$

where p represents the force which does differential work during a differential displacement $d\delta$. Moreover, the maximum force exerted to the tube, P_{max}, can be obtained from the *F-D* diagram, directly.

6. Validation of Results

To verify the presented finite element modeling, the axial crush of a sample hybrid tube which is reported by El-Hage et al. [14] was modeled and results were compared. As figure 5 shows, there is a good agreement between the present study and the Ref. [14].

It is to be noted here that, the present modeling procedure is verified using data of the two-layered hybrid tube (2L45SH) reported by El-Hage et al. [14]. Therefore, similar to what Ref. [14] has considered, this verification sample is likewise modeled supposing and modeling a 45 degree chamfer to initiate folding. Comparing with numerical and experimental results reported by Ref. [14], present models are validated and numerical results are enough reliable. Therefore, this 45 degree chamfer is not replaced with a buckling initiator in the verification sample. However, other case-study samples (unlike the verification sample) include a circumferential depression of a row of elements as a buckling initiator (which is only a geometrical parameter) in order to initiate folding and lead its pattern.
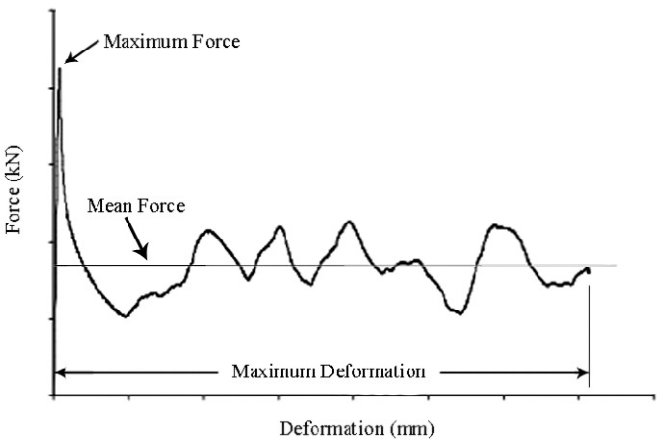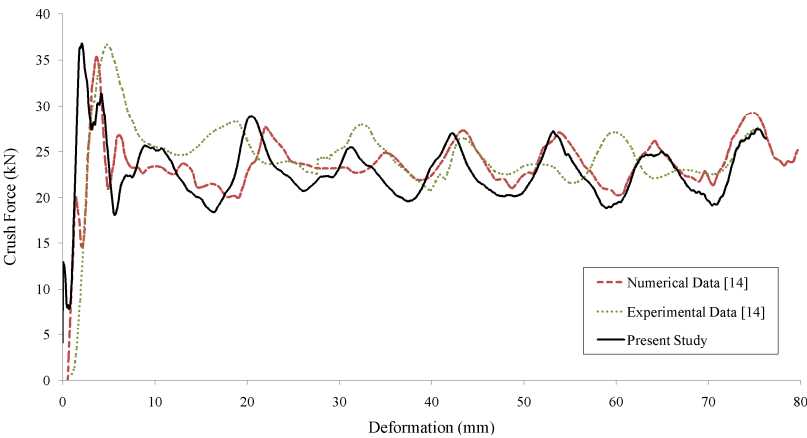
Fig4. A sample F-D diagram

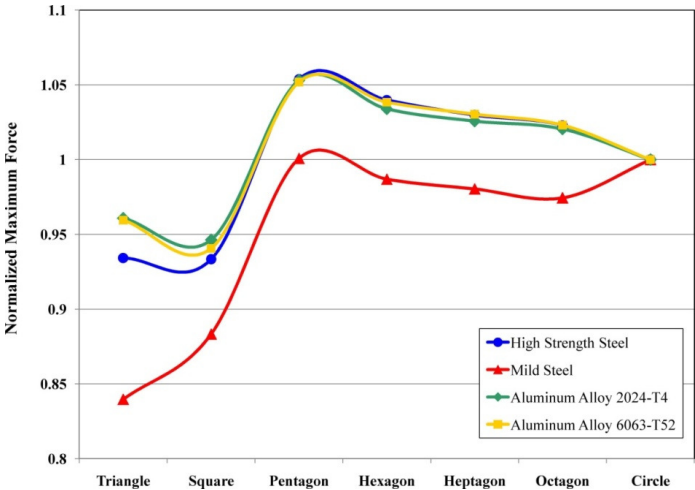**Fig5.** Comparison of the results of present model and Ref. [14]

Fig6. Effects of cross-section shape and material properties on normalized maximum forces in metallic tubes
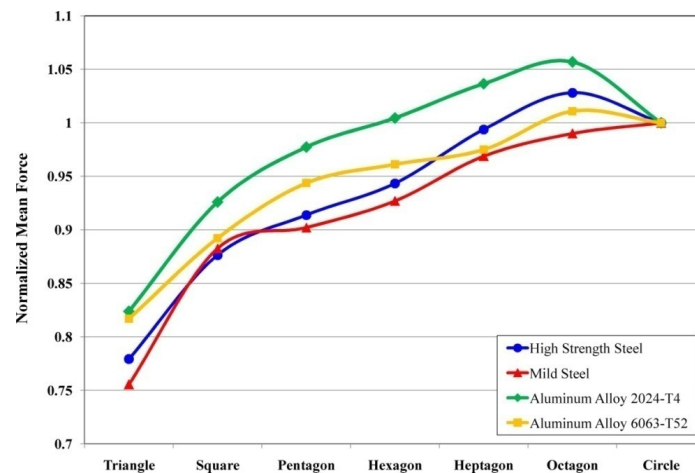
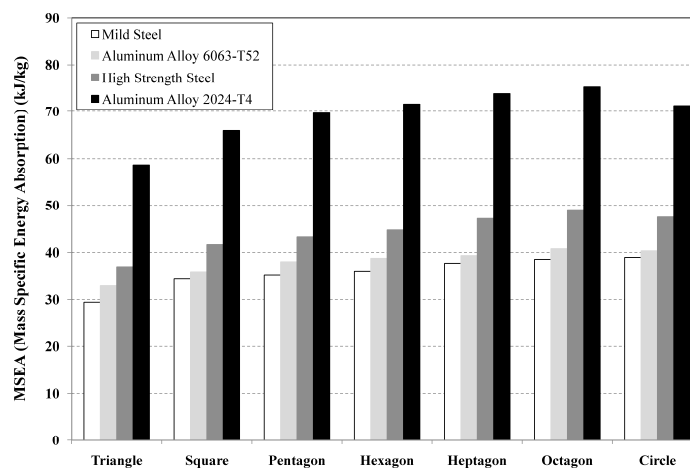**Fig7.** Effects of cross-section shape and material properties on normalized mean forces in metallic tubes

Fig8. Effects of cross-section shape and material properties on the MSEA in metallic tubes

7. Results and Discussion

Results of simulations, including the MSEA and the normalized maximum and mean forces for the metallic tubes are presented in figures 6, 7, and 8. Note that, all forces are normalized with respect to forces obtained from corresponding circular-shaped ones.

As shown in figures 6 and 7, the mean and maximum forces of high strength steel tubes are more than those of mild steel ones. Hence, for equal Young's module, higher strength yields greater maximum and mean forces for metal tubes. Moreover, figures 6 and 7 show that, the mean and maximum forces for mild steel tubes are more than those of aluminum alloy ones. This means for equal strengths, higher Young's Modulus yields higher maximum and mean forces.

Since the mean force is the absorbed energy per unit deformed length, and also all tubes have identical deformed lengths, the mean forces, indeed, represent the total absorbed energy. Thus, it can be concluded that a material with higher strength and Young's modulus can absorb more energy.

On the other hand, according to figure 8, the mass specific energy absorbing capability of the AA 2024-T4 tubes is significantly higher than others because of their lower density or equivalently higher strength to weight ratio. The MSEAs obtained for AA 6063-T52 tubes, can be linked to its lower strength, seem to be smaller than those of other aluminum alloy tubes.

As illustrated in figures 9 to 11, results of simulations for hybrid tubes are compared with metallic tube (without the composite overlay). Note that, all forces are normalized with respect to the forces obtained from corresponding circular-shaped ones.
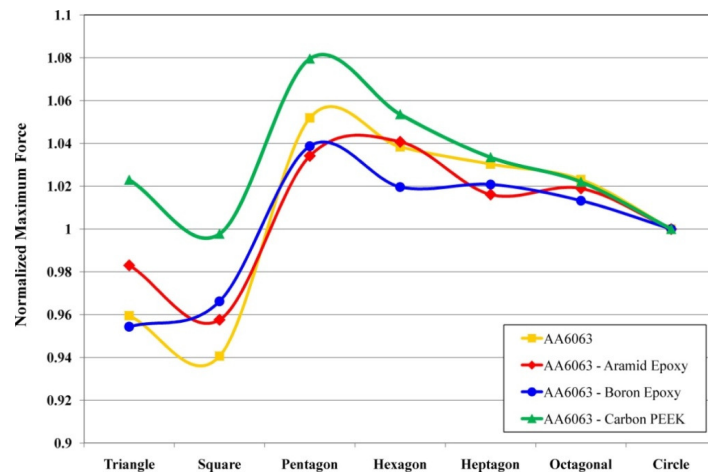
Fig9. Effects of cross-section shape and material properties on normalized maximum forces in hybrid tubes
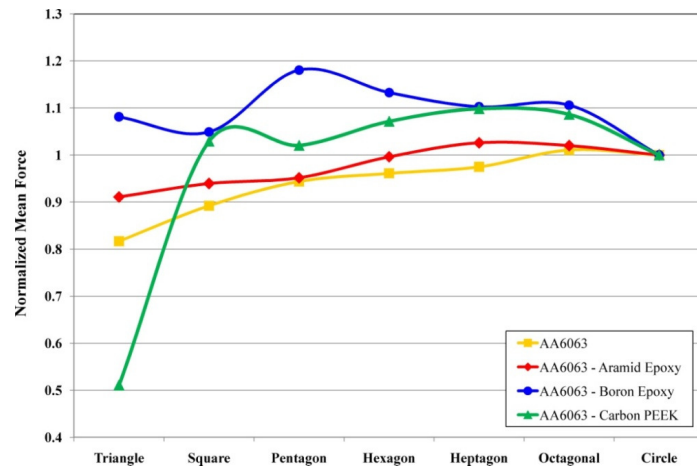

Fig10. Effects of cross-section shape and material properties on normalized mean forces in hybrid tubes
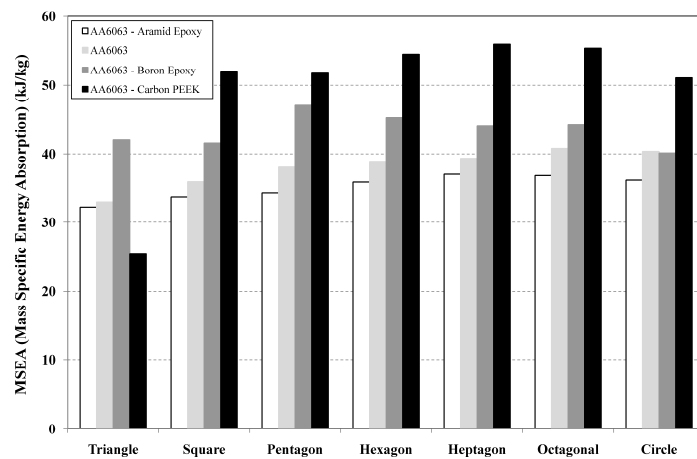

Fig11. Effects of cross-section shape and material properties on the MSEA in hybrid tubes
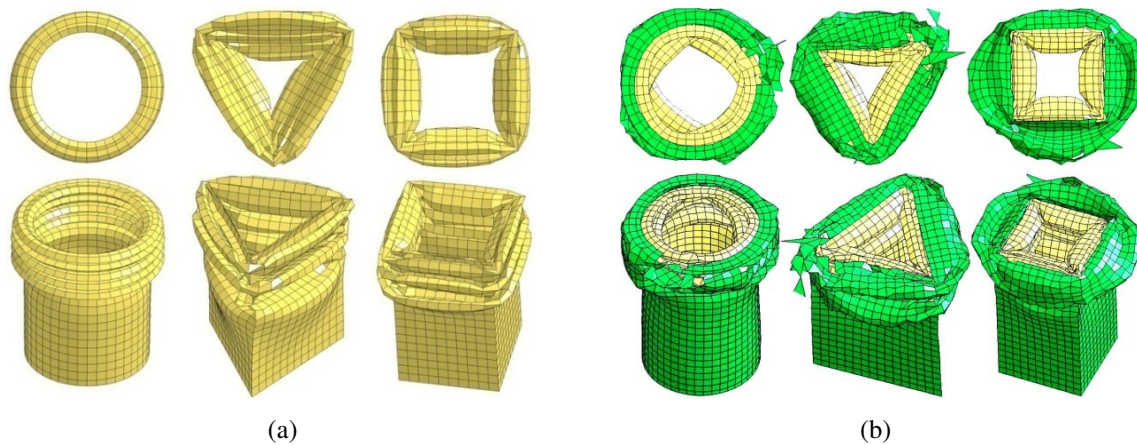
(a)   (b)

Fig12. Samples of deformed tubes, (a) metallic tube and (b) hybrid tube
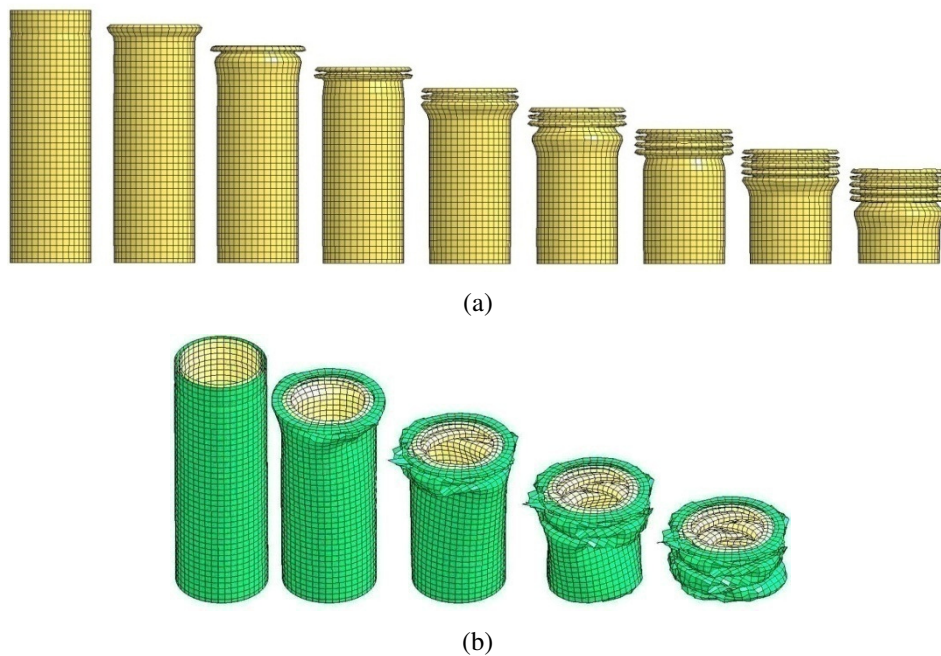

(a)

(b)

Fig13. Folding process for a sample, (a) metallic tube and (b) hybrid tube

As mentioned before, the carbon PEEK overlays have almost the average mechanical properties in comparison with two other composite laminates. Although the longitudinal tensile strength of Aramid epoxy is more than others; its longitudinal Young's modulus and longitudinal compressive strength, which may play the most important rules in the energy absorption, are very small in comparison with other composite laminas. As figures 9 and 10 illustrate, the maximum and mean forces of almost all hybrid tubes are more than metallic ones.

Figure 11 demonstrates that the Aramid epoxy hybrid tubes are weaker even than the metallic ones.

On the other hand, carbon PEEK and Boron epoxy hybrid tubes have significantly higher mass specific energy absorbing capability in comparison with metallic tubes. However, carbon epoxy hybrid tubes (with almost average mechanical properties) have the best MSEA as well as maximum and mean forces.

As shown in figures 8 and 11, in these groups of metallic and hybrid tubes, there are cross-section shapes, which yield higher MSEA, even more than the circle shape. This fact indicates that the metallic tubes with heptagon and octagon shapes can absorb the crush energy nearly 6% more than the circular tubes. Similarly, the hybrid ones with the heptagonal

and octagonal cross section shape can absorb the crushing energy almost 10% more than circle-shaped one. This indicates that some non-circular cross-section shaped tubes with higher efficiencies can be found, which have more effective roles during crush.

Three samples of deformed metallic and hybrid tubes are presented in figure 12. Moreover, the folding processes of metallic and hybrid tubes with circular cross-sections are shown in figure 13. As it can be seen in figures 12 and 13, although different buckling modes and folding patterns exist for several shapes of metallic tubes, all of them are neat and regular in shape. While, the composite overlays crumble during the impact because of their brittle nature. This brittle behavior of composite overlays, which can be considered as an external restrictive condition caused by the contact conditions defined between the layers, may affect the folding patterns of metallic tubes which they cover.

8. Conclusion

In this paper, the axial crush of metallic and hybrid energy absorbing thin-walled tubes with various cross-sections and material properties is investigated using finite element software LS-DYNA. The main objective of this study is to understand the combined effects of material properties and cross-section shapes on the crushing behavior of thin-walled tubes.

The results obtained for the metallic energy absorbing thin-walled tubes shows that although the strength and Young's modulus have developing effects on the crush behavior, the MSEA significantly depends on the strength to weight ratio. Moreover, it can be concluded that, by correct reinforcing the metallic tubes with composite laminates, the mass specific energy absorption and also other crush behaviors can be significantly improved.

Furthermore, it can be concluded that, some polygonal shapes with better crush behavior, even 10% better than the circular ones, can be achieved. As illustrated in this paper, hybriding thin-walled tubes can considerably improve their structural behavior due to their higher strength to weight ratio, and as a result, this kind of tubes can absorb more energy per unit of their deformed mass than common metallic tubes.

REFERENCES

[1]. Abramowicz, W., Jones, N., Dynamic axial crushing of circular tubes, International Journal of Impact Engineering 2 (1984a) 263-281.

[2]. Abramowicz, W., Jones, N., Dynamic axial crushing of square tubes, International Journal of Impact Engineering 2 (1984b) 179-208.

[3]. Abramowicz, W., Jones, N., Dynamic progressive buckling of circular and square tubes, International Journal of Impact Engineering 4 (1986) 243-270.

[4]. Al Galib, D., Limam, A., Experimental and numerical investigation of static and dynamic axial crushing of circular aluminum tubes, Thin-Walled Structures 42 (2004) 1103-1137.

[5]. Tai, Y.S., Huang, M.Y., Hu, H.T., Axial compression and energy absorption characteristics of high-strength thin-walled cylinders under impact load, Theoretical and Applied Fracture Mechanics 53 (2010) 1-8.

[6]. Mamalis, A.G., Manolakos, D.E., Demosthenous, G.A., Johnson, W., Axial plastic collapse of thin bi-material tubes as energy dissipating systems, International Journal of Impact Engineering 11 (1991) 185-196.

[7]. Shin, K.Ch., Lee, J.J., Kim, K.H., Song, M.Ch., Huh, J.S., Axial crush and bending collapse of an aluminum/GFRP hybrid square tube and its energy absorption capability, Composite Structure 57 (2002) 279-287.

[8]. Thuis, H.G.S.J., Metz, V.H., The influence of trigger configurations and laminate lay-up on the failure mode of composite crush cylinders, Composite Structure 25 (1993) 37-43.

[9]. Yang, Y., Nakai, A., Hamada, H., Effect of collapse trigger mechanisms on the energy absorption capability of FRP tubes, 16th International Conference on Composite Materials (2007).

[10]. Sultan Aljibori, H.S., Mahdi, E., Hamouda, A.M., Mokhtar, A.S., Non-linear dynamic analysis of composite conical shell structures, International Journal of Engineering & Technology 9:9 (2009) 411-422.

[11]. Huang, J., Wang, X., Numerical and experimental investigations on axial crushing response of composite tubes, Composite Structures 91 (2009) 222-228.

[12]. Ghasemnejad, H., Hadavinia, H., Aboutorabi, A., Effect of delamination failure in crashworthiness analysis of hybrid composite box structures, Materials and Design 31 (2010) 1105-1116.

[13]. El-Hage, H., Mallick, P.K., Zamani, N., A numerical study on the quasi-static axial crush characteristics of square aluminum tubes with chamfering and other triggering mechanisms, International Journal of Crashworthiness 10:2 (2005) 183-196.

[14]. El-Hage, H., Mallick, P. K., Zamani, N., Numerical modeling of quasi-static axial crush of square aluminum-composite hybrid tubes, International Journal of Crashworthiness 9:6 (2004) 653-664.

[15]. LS-DYNA User's Manual, Livermore Software Technology Corporation (LSTC), 2010.

[16]. Illg, W., McEvily, A.J., Technical Note 3994, National Advisory Committee for Aeronautics (NACA), 1957.

[17]. Vasiliev, V.V., Morozov, E.V., Mechanics and Analysis of Composite Materials, Elsevier Science Ltd., 2001.

[18]. Han, H., Taheri, F., Pegg, N., Lu, Y., A numerical study on the axial crushing response of hybrid pultruded and ±45º braided tubes, Composite Structures 80 (2007) 253-264.